Constraints on the identity of the dark matter from strong gravitational lenses

Ran Li[1]⋆, Carlos S. Frenk[2], Shaun Cole[2], Liang Gao[1], Sownak Bose[2], Wojciech A. Hellwing[3,4]

[1]*Key laboratory for Computational Astrophysics, Partner Group of the Max Planck Institute for Astrophysics,*
National Astronomical Observatories, Chinese Academy of Sciences, Beijing, 100012, China
[2]*Institute for Computational Cosmology, Department of Physics, University of Durham, South Road, Durham, DH1 3LE*
[3]*Institute of Cosmology and Gravitation, University of Portsmouth, Burnaby Road, Portsmouth PO1 3FX*
[4]*Interdisciplinary Centre for Mathematical and Computational Modelling (ICM), University of Warsaw, ul. Pawińskiego 5a, Warsaw, Poland*

12 May 2022

ABSTRACT
The cold dark matter (CDM) cosmological model unambigously predicts that a large number of haloes should survive as subhaloes when they are accreted into a larger halo. The CDM model would be ruled out if such substructures were shown not to exist. By contrast, if the dark matter consists of warm particles (WDM), then below a threshold mass that depends on the particle mass far fewer substructures would be present. Finding subhaloes below a certain mass would then rule out warm particle masses below some value. Strong gravitational lensing provides a clean method to measure the subhalo mass function through distortions in the structure of Einstein rings and giant arcs. Using mock lensing observations constructed from high-resolution N-body simulations, we show that measurements of approximately 20 strong lens systems with a detection limit of $M_{\rm low} = 10^7 h^{-1} {\rm M}_\odot$ would clearly distinguish CDM from WDM in the case where this consists of 7 keV sterile neutrinos such as those that might be responsible for the 3.5 keV X-ray emission line recently detected in galaxies and clusters.

1 INTRODUCTION

A variety of observations indicate that dark matter accounts for more than 80% of the mass content of the Universe and so it dominates the gravitational evolution of cosmic structure. Its existence is inferred through its gravitational effects in galaxies and clusters and through the distortion of galaxy images by gravitational lensing (for a recent review see Frenk & White 2012). Measurements of temperature anisotropies in the cosmic microwave background (CMB; e.g. Planck Collaboration et al. 2014) show that the dark matter is not baryonic (e.g. Planck Collaboration et al. 2014) but its identity remains unknown.

The CDM model in which the dark matter consists of cold collisionless elementary particles (i.e. with negligible thermal velocities in the early universe), such as the lightest stable supersymmetric particle, has been shown, over the past 30 years, to provide an excellent match to a variety of observations, many of them predicted in advance of the measurements. These include the structure of the CMB temperature anisotropies (Peebles 1982; Planck Collaboration et al. 2014) and the pattern of galaxy clustering (Davis et al. 1985; Springel 2005; Tegmark et al. 2004; Cole et al. 2005, see Frenk & White 2012 for a comprehensive list of references). There are claims that the CDM particles may have already been detected through γ-ray annihilation radiation

from the Galactic Centre (Hooper & Goodenough 2011) but these are controversial; the LHC has not yet turned out any evidence for supersymmetry.

The warm dark matter (WDM) model, in which the particles had non-negligible thermal velocities at early times, is a viable alternative to CDM. Indeed, there are also claims that such particles may have been detected, in this case through particle decays resulting in the 3.5 keV X-ray line recently discovered in galaxies and galaxies clusters (Boyarsky et al. 2014; Bulbul et al. 2014). A 7 keV sterile neutrino originally introduced to explain neutrino flavour oscillations (Boyarsky et al. 2009) could be such a particle. However, these claims are also controversial (c.f. Riemer-Sorensen 2014).

A very attractive feature of both the CDM and WDM models is that they have predictive power; both are eminently falsifiable. The major difference between them stems from the free-streaming cutoff in the primordial power spectrum of density fluctuations which, in the case of keV-mass particles, occurs on the mass scale of dwarf galaxies whereas, in the case of cold particles, it occurs on the scale of planets. Thus, on scales larger than individual bright galaxies, CDM and WDM are almost indistinguishable, but on subgalactic scales they make radically different predictions.

The most striking difference between CDM and WDM is

the halo mass function which turns over at the very different cutoff mass scales of the two models. The halo mass function itself is difficult to measure directly but, as we shall see in this paper, the mass function of subhaloes (that is haloes that have been accreted into a larger halo and survive) is accessible through observations. Rigorous and reliable predictions for the halo and subhalo mass functions in CDM and WDM exist from high-resolution N-body simulations (Springel et al. 2008; Gao et al. 2011; Colín et al. 2000; Avila-Reese et al. 2003; Lovell et al. 2012, 2014; Hellwing et al. 2015; Cautun et al. 2014; Bose et al. 2015).

Gravitational lensing provides an ideal tool to measure the subhalo mass function (SHMF). Distinguishing keV-mass WDM from CDM requires measuring this function below a mass of $\sim 10^9 \ h^{-1} \mathrm{M}_\odot$. This mass limit may be inaccessible to measurements of weak lensing (e.g. Li et al. 2013, 2014), but it is well within the range of strong lensing measurements of massive galaxies. The presence of subhaloes in the central regions of galactic haloes can perturb the flux ratio of multi-image systems (e.g. Kochanek 1991; Mao & Schneider 1998; Metcalf & Madau 2001). It can also distort the images of extended giant arcs or Einstein rings (e.g. Koopmans 2005; Vegetti & Koopmans 2009a; Vegetti et al. 2012).

Flux ratio anomalies have been measured only for a handful of quasars and appear to reveal more small-scale structure than predicted even for CDM, possibly due to projection effects from intervening haloes and to inaccurate modelling of the complex mass distribution in the lens galaxy (e.g. Xu et al. 2009, 2015). For example, Hsueh et al. (2015) have shown that the flux ratio anomaly of CLASS B1555+375, one of the most anomalous lens systems known, can be explained by the presence of a previously undetected edge-on disk in the lens galaxy.

Distortions of Einstein rings or giant arcs could offer a more direct method. The technique developed by Koopmans (2005) and Vegetti & Koopmans (2009a) can detect individual subhaloes and, using the Bayesian formalism of Vegetti & Koopmans (2009b), a sample of detections can constrain the SHMF. Vegetti et al. (2014) analyzed 11 strong lenses in the Sloan Lens ACS Survey (Bolton et al. 2006) and obtained one detection in SDSS J0956+5110. Their estimate of the projected substructure mass fraction (i.e. the normalisation of the SHMF) is in agreement with CDM and is lower than the values inferred from flux ratio anomalies. However, the constraints on the slope of the SHMF derived from such a small sample are weak. Many more strong lenses will become available with future galaxy surveys such as Euclid and LSST.

In this work we investigate how the detection of subhaloes in perturbed Einstein rings or giant arcs can be used to distinguish the SHMF in CDM and WDM. For this we make use of the high-resolution CDM and WDM simulations of the Copernicus Complexio (COCO) project (Hellwing et al. 2015; Bose et al. 2015). The COCO-WARM simulation had an initial power spectrum appropriate to a thermal WDM particle of 3.3 keV. It turns out that this power spectrum provides a very good approximation to that of the coldest possible sterile neutrino model that is compatible with the decay interpretation of the 3.5 keV X-ray line (corresponding to a value of the lepton asymmetry parameter, $L_6 = 8.66$ Lovell et al. 2015; Bose et al. 2015). Thus, ruling out this

particular model would exclude the entire family of 7 keV sterile neutrinos.

The paper is organized as follows. In Section 2 we briefly introduce the COCO project. In Section 3 we estimate the probability of detecting subhaloes in dark matter halo centres. In Section 4 we present the modelling formalism of subhalo detections. In Section 5 we show the constraining power of subhalo detection from multiple lens systems on the SHMF. Our conclusions are summarized in Section 6

2 SIMULATION DATA

We use the COCO simulations to derive the SHMF in a WDM universe. We begin by providing a brief discussion of the COCO simulations.

2.1 *Copernicus Complexio* simulations

The *COpernicus COmplexio* simulations (Hellwing et al. 2015), carried out by the *Virgo Consortium*, consist of a set of cosmological zoom-in simulations performed with a modified version of the Gadget-3 code (Springel et al. 2001; Springel 2005). The region for resimulation was extracted from the *Copernicus Complexio Low Resolution* (COLOR) simulation (a periodic cubic volume of side $70.4h^{-1}\mathrm{Mpc}$); it contains 12.9 billion high resolution particles in a roughly spherical region of radius $17.4h^{-1}\mathrm{Mpc}$. Each of the high-resolution dark matter particles has a mass of $1.135 \times 10^5 h^{-1}\mathrm{M}_\odot$. The gravitational softening was kept fixed at $230h^{-1}\mathrm{pc}$ in comoving unit. Both COCO and COLOR assume the WMAP-7 cosmological parameters (Komatsu et al. 2010): $\Omega_\mathrm{m} = 0.272$, $\Omega_\Lambda = 0.728$, $h = 0.704$, $n_\mathrm{s} = 0.968$ and $\sigma_8 = 0.81$.

Simulations were performed for both a CDM and a 3.3 keV WDM universe: COCO-COLD and COCO-WARM respectively. The initial conditions for both sets were arranged to have the same Fourier phases and were generated using the method developed by Jenkins (2013).

The effect of free streaming at early times is to impose a cutoff in the power spectrum. This is imposed in the initial conditions for COCO-WARM, through a modified transfer function, $T(k)$, so that the power spectrum for WDM is related to that for CDM by:

$$P_\mathrm{WDM}(k) = T^2(k) P_\mathrm{CDM}(k) \,, \qquad (1)$$

where $T(k)$ is given by the fitting formula of (Bode et al. 2001):

$$T(k) = (1 + (\alpha k)^{2\nu})^{-5/\nu} \,, \qquad (2)$$

where the constant, $\nu = 1.12$, and α depends on the WDM particle mass, m_WDM, as

$$\alpha = 0.049 \left(\frac{m_\mathrm{WDM}}{\mathrm{keV}}\right)^{-1.11} \left(\frac{\Omega_\mathrm{WDM}}{0.25}\right)^{0.11} \left(\frac{h}{0.7}\right) h^{-1}\mathrm{Mpc} \qquad (3)$$

(Viel et al. 2005). The smaller the WDM particle mass, the larger the cutoff scale in the power spectrum cutoff. In COCO-WARM the equivalent thermal particle mass is $m_\mathrm{WDM} = 3.3$ keV. As discussed in the introduction, this power spectrum is a very good approximation to the power spectrum

of the coldest possible sterile neutrino model that is compatible with the decay interpretation of the recently measured 3.5 keV X-ray line (corresponding to a value of the lepton asymmetry parameter, $L_6 = 8.66$; Lovell et al. 2015; Bose et al. 2015). This power spectrum leads to a delay in the formation epoch of haloes of mass below $\sim 2 \times 10^9 h^{-1} M_\odot$ in COCO-WARM relative to COCO-COLD (Bose et al. 2015). We refer the reader to Bose et al. (2015) and Hellwing et al. (2015) for further details of the COCO simulations.

2.2 Subhaloes in COCO-WARM and COCO-COLD

Haloes in the COCO simulations were identified using the FOF algorithm (Davis et al. 1985) with a linking length of 0.2 times the mean interparticle separation. Gravitationally-bound subhaloes within each halo were identified using the SUBFIND algorithm (Springel et al. 2001). Since the initial conditions for both COCO-WARM and COCO-COLD had the same initial Fourier phases, any differences in the abundance of low mass subhaloes between the two are due entirely to the different input power spectra.

In order to obtain the true mass function in WDM simulations, it is necessary to identify and exclude artificial haloes that form in N-body simulations from initial power spectra with a resolved cutoff, as is the case for COCO-WARM. These spurious, small-mass haloes are generated by discreetness effects that cause fragmentation of filaments, as discussed by Wang & White (2007) in the context of simulations from hot dark matter initial conditions. The same phenomenon is seen in WDM simulations (Angulo et al. 2013; Lovell et al. 2014; Bose et al. 2015). Wang & White (2007) found that a large fraction of these spurious haloes can be removed by eliminating haloes with mass below,

$$M_{\mathrm{lim}} = 10.1 \, \bar{\rho} \, d \, k_{\mathrm{peak}}^{-2} \,, \qquad (4)$$

where d is the mean interparticle separation and k_{peak} the wavenumber at which the dimensionless power spectrum, $\Delta(k)^2 = k^3 P(k)$, reaches its maximum. Spurious haloes can also be identified by tracing back their particles to the (unperturbed) initial density field. The Lagrangian regions from which spurious haloes form tend to be much flatter that the corresponding region for genuine haloes (Lovell et al. 2014). By calculating the inertia tensor of the initial particle load, the sphericity of a halo can be defined as c/a, where a^2 and c^2 are the largest and smallest eigenvalues of the inertia tensor. Spurious haloes in the COCO-WARM catalogues were removed by Bose et al. (2015) by eliminating all haloes with $s_{\mathrm{half-max}} < 0.165$ and $M_{\mathrm{max}} < 0.5 M_{\mathrm{lim}}$, where $s_{\mathrm{half-max}}$ is the sphericity of the halo at the half-maximum mass snapshot and M_{max} is the maximum mass a halo achieved during its growth history. We refer the reader to Lovell et al. (2014) and Bose et al. (2015) for a detailed discussion of these criteria.

In Fig. 1, we show the differential subhalo mass function (SHMF) within host haloes in different mass bins. The SHMF in COCO-COLD can be fitted by the power law, $n(M) \equiv dN(< M_{\mathrm{sub}})/dM = A_0 M^{-\alpha}$, where $N(< M_{\mathrm{sub}})$ is the total number of subhaloes with mass smaller than M_{sub} and $\alpha = 1.9$ (Springel et al. 2008; Gao et al. 2012). The COCO-WARM simulation produces similar numbers of subhaloes as COCO-COLD at larger masses but much smaller
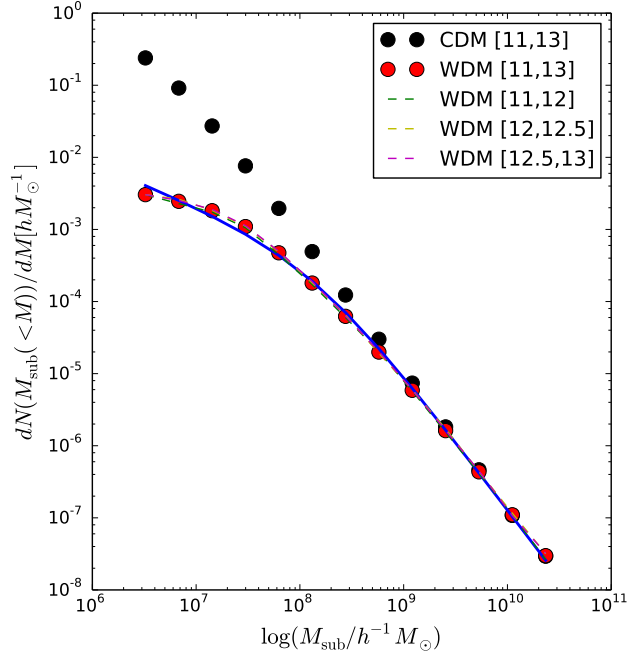
Figure 1. The differential subhalo mass function for host haloes of different mass. The solid black (COCO-COLD) and red (COCO-WARM) points show the subhalo mass function for host haloes with mass in range $[10^{11} h^{-1} M_\odot, 10^{13} h^{-1} M_\odot]$. The dashed lines show the mass function for haloes in different mass ranges in COCO-WARM. We scale the dashed lines to match the red solid points (by requiring the average amplitude of different curves to be the same), so that one can compare the shape of the subhalo mass functions in COCO-WARM. The blue line shows the fit to the SHMF in COCO-WARM.

numbers for $M_{\mathrm{sub}} > 10^9 h^{-1} M_\odot$. The slope of the SHMF in COCO-WARM begins to deviate appreciably from $\alpha = 1.9$ at $\sim 10^8 h^{-1} M_\odot$. At at $10^7 h^{-1} M_\odot$, the difference between the two SHMFs has grown to be a factor of 10. We fit the subhalo mass function in COCO-WARM with the expression used by Schneider et al. (2012):

$$n_{\mathrm{WDM}}/n_{\mathrm{CDM}} = (1 + m_c/m)^{-\beta} \,. \qquad (5)$$

Lovell et al. (2014) show that the WDM mass function is well fit adopting $\beta = 1.3$. We fix $\beta = 1.3$ and fit the mass function of COCO-WARM to find a best-fit value of $m_c = 1.3 \times 10^8 h^{-1} M_\odot$. The corresponding fit is shown by the solid lines in the Fig. 1.

3 SUBSTRUCTURE DETECTION IN STRONG GRAVITATIONAL LENSES

If the projected position of a subhalo is close to the Einstein radius of a strong lens system, it can perturb the surface brightness distribution of the Einstein ring. The strength of the perturbation depends on the mass of the subhalo and its relative distance to the Einstein ring.

To investigate the probability of a subhalo falling in the region of an Einstein ring, we first calculate the Einstein

radius of dark matter haloes of a given mass. In the real Universe, the size of the Einstein radius is determined by the central mass distribution which, in sufficiently large haloes, is dominated by the baryonic component of the galaxy. Previous analyses have shown that modelling the total central mass distribution as a singular-isothermal-sphere (SIS) can successfully predict the location of strong lensing images (e.g. Koopmans et al. 2006; Gerhard et al. 2001; Czoske et al. 2008).

Denoting the stellar velocity dispersion as σ_v, the Einstein radius of a SIS can be written as:

$$\theta_E = \frac{4\pi\sigma_v^2}{c^2}\frac{D_{\rm l,s}}{D_{\rm s}},\qquad(6)$$

where $D_{\rm s}$ is the angular diameter distance from the source to the observer and $D_{\rm l,s}$ is the distance between the lens and the source. Since COCO is a set of dark matter-only simulations, it provides halo masses but not stellar velocity dispersions. A convenient way to infer the latter is to take them from the stellar velocity-dispersion *vs* halo-mass relation obtained in a realistic cosmological hydrodynamics simulation. Here we use the recent EAGLE reference simulation which follows the coupled evolution of baryons and dark matter in a cubic volume of side 100 Mpc, with gas mass resolution of $1.8 \times 10^6 {\rm M_\odot}$ and softening length of 0.7 kpc (Schaye et al. 2015). EAGLE provides a good match to both the observed stellar mass function and the galaxy size-stellar mass relation so it is reasonable to assume that the stellar velocity dispersions are also realistic. Using the public EAGLE database[1] (McAlpine et al. 2015), we find that the velocity-dispersion *vs* halo-mass relation is well fit by:

$$\sigma_v = \sigma_0\frac{(M/M_1)^{\gamma_1}}{(1+M/M_1)^{\gamma_2-\gamma_1}},\qquad(7)$$

where M is the halo mass, $\sigma_0 = 117$ km s^{-1}, $M_1 = 1.5 \times 10^{12}h^{-1}{\rm M_\odot}$, $\gamma_1 = 4.30$, $\gamma_2 = 6.79$, and σ_v is the average stellar velocity dispersion within the inner 5 kpc of the central galaxy.

Vegetti et al. (2014) have shown that the probability of detecting a substructure in an Einstein ring depends on the mass and position of the subhalo and on the gradient of the surface brightness distribution of the lensed galaxy. In this work, we adopt the simple assumption that within a thin region around the Einstein ring, any subhalo of mass larger than a threshold, $M_{\rm low}$, can be detected through its perturbation to the Einstein ring (Vegetti & Koopmans 2009b). In a forthcoming paper we will investigate the effect of a more realistic sensitivity function based on the results of Vegetti et al. (2014). Following Vegetti & Koopmans (2009b), we take the width of this thin annulus to be $\Delta\theta = 0.3$ arcsec.

The dark matter mass contained in the Einstein ring, $M_{\rm ring}$, is given by:

$$M_{\rm ring}(R_E) = \int_{R_E-\Delta R}^{R_E+\Delta R} 2\pi R\,\Sigma_{\rm dm}(R)\,dR,\qquad(8)$$

where the Einstein radius, $R_E = \theta_E D_{\rm l}$; $\Sigma_{\rm dm}(R)$ is the surface mass density of the dark matter halo; and $\Delta R = \Delta\theta D_{\rm l}$.

From Eq.5, the probability of finding a subhalo of mass, m, per unit volume can be written as:

$$\left.\frac{dP}{dm}\right|_{\rm true} = A_0 m^\alpha (1+m_c/m)^{-\beta},\qquad(9)$$

where for COCO-WARM, we have $\beta=1.3$ and $m_c = 1.3 \times 10^8 h^{-1}{\rm M_\odot}$, whereas for COCO-COLD, $m_c = 0$.

We denote the maximum and the minimum mass of the subhaloes of interest that lie within the Einstein ring region as $M_{\rm max}$ and $M_{\rm min}$ respectively and adopt $M_{\rm max} = 10^{10}h^{-1}{\rm M_\odot}$ and $M_{\rm min} = 10^6 h^{-1}{\rm M_\odot}$. We can then define a normalization factor, A_0, as:

$$A_0 = \frac{1}{\int_{M_{\rm min}}^{M_{\rm max}} m^\alpha(1+m_c/m)^{-\beta}dm}.\qquad(10)$$

The expectation value of the number of subhaloes in the Einstein ring region with mass $M_{\rm min} < m < M_{\rm max}$ can then be written as:

$$\mu_0(\alpha,\beta,m_{\rm c},f_E,M_{rmring}) = \frac{f_E M_{\rm ring}}{\int_{M_{\rm min}}^{M_{\rm max}} m\left.\frac{dP}{dm}\right|_{\rm true}dm},\qquad(11)$$

where $f_E = f_{\rm sub}(R_E)$ and $f_{\rm sub}$ is the fraction of mass contained in subhaloes at a projected radius R.

When a halo merges into a larger system and becomes a subhalo, it experiences dynamical friction and tidal striping. Subhaloes spiral into the centre of the host halo and loose mass and many of them are completely disrupted. As a result, we expect the fraction of mass contained in subhaloes to increase with projected radius. The COCO volume contains only a few dark matter haloes of mass larger than $10^{13}h^{-1}$Mpc, making the estimation of $f_{\rm sub}$ noisy. We therefore make use of the analytical formula for $f_{\rm sub}(R)$ derived by Han et al. (2015). For dark matter haloes of mass in the range $[10^{13}, 10^{14}]$ $h^{-1}{\rm M_\odot}$, $f_{\rm sub}$ can be approximated as:

$$f_{\rm sub} = 0.35(R/r_{\rm vir})^{1.17},\qquad(12)$$

where $r_{\rm vir}$ is the virial radius of the halo and R the projected radius.

Observationally, it is only possible to detect subhaloes more massive than a certain threshold. Vegetti & Koopmans (2009b) found the measurement errors on subhalo mass to be approximately Gaussian distributed with standard deviation, σ_m. In our catalogues, we will consider as 'detected subhaloes' those having a measured mass larger than $M_{\rm low} \equiv 3\sigma_m$. We note that this definition is different from that adopted by Vegetti et al. (2014), who empolyed a detection threshold derived from the probability density of a substructure mass, given the observed lensed data, marginalised over the host lens and background source parameters.

Taking into account the detectability of a subhalo, we can rewrite the expected number of subhaloes in the Einstein ring region as:

$$\mu(\alpha,\beta,m_c,f_E,M_{\rm ring}) =$$
$$\mu_0\int_{M_{\rm low}}^{M_{\rm max}}\int_{M_{\rm min}}^{M_{\rm max}}\left.\frac{dP}{dm}\right|_{\rm true}\exp\left[\frac{(m-m')^2}{2\sigma_m^2}\right]dm'dm.\qquad(13)$$

We generate mock subhalo detection events using a Monte Carlo method. Firstly, we randomly sample N haloes with mass in the range $[10^{13}, 10^{14}]$ $h^{-1}{\rm M_\odot}$ using the mass function of the EAGLE reference simulation. This mass range is consistent with the lens sample in the Sloan Lens ACS Survey (SLAC) (Vegetti et al. 2014). For simplicity, we assume

that for all the strong lens systems, $z_l = 0.3$ and $z_s = 0.5$, comparable to the values in the SLAC observations.

Using Eq.6-7, we calculate the Einstein radius for each halo, and the corresponding mass contained within each ring, M_{ring}. We assume that the appearance of a subhalo follows a Poisson distribution with expectation $\mu(\alpha, \beta, m_c, f_E, M_{ring})$. We then sample the subhaloes according to Eq. 9 assuming a Gaussian measurement error with standard deviation, σ_m, for each subhalo.

To date, the smallest subhalo mass measured using this technique is $1.9 \pm 0.1 \times 10^8 M_\odot$, detected with a significance of 12σ (Vegetti et al. 2012). In this study, we consider two values for the minimum detection threshold, M_{low}: $10^8 h^{-1} M_\odot$, the limit of current observations, and $10^7 h^{-1} M_\odot$, our optimistic expectation for future observations. We generate mock datasets for both CDM and WDM with $N = 20, 100$ and 1000 host haloes with Einstein rings.

4 BAYESIAN INTERFERENCE FOR SUBHALO DETECTIONS

The differences in subhalo detection rates can be interpreted quantitatively using Bayesian theory. Here, we follow the formalism developed by Vegetti & Koopmans (2009b), outlined below.

Assuming that subhaloes follow a Poisson distribution in a lens system, the likelihood of finding n_s subhaloes of mass, $\mathbf{m}$, in an Einstein ring system can be written as:

$$\mathcal{L}(n_s, \mathbf{m}|\mathbf{p}, \mathbf{q}) = \frac{e^{-\mu} \mu^{n_s}}{n_s!} \prod_{i=1}^{n_s} P(m_i|\mathbf{p}, \mathbf{q}), \qquad (14)$$

where the vector, $\mathbf{q} = \{\alpha, f_E, M_{ring}, \beta, m_c\}$, gives the parameters of the model and the vector, $\mathbf{p} = \{M_{min}, M_{max}, M_{low}\}$, contains the fixed values of the parameters that define the minimum and maximum mass allowed by the subhalo mass function and the threshold detection limit of a given observation. If the errors on the measurement of subhalo mass are Gaussian distributed with standard deviation, σ_m, $P(m_i|\mathbf{p}, \mathbf{q})$ gives the probability of finding a subhalo with detected mass, m_i, given the true subhalo mass distribution function, $\left.\frac{dP}{dm}\right|_{true}$.

$$P(m_i|\mathbf{p}, \mathbf{q}) = \frac{\int_{M_{min}}^{M_{max}} \left.\frac{dP}{dm}\right|_{true} \exp\left[\frac{(m_i - m')^2}{2\sigma_m^2}\right] dm'}{\int_{M_{low}}^{M_{max}} \int_{M_{min}}^{M_{max}} \left.\frac{dP}{dm}\right|_{true} \exp\left[\frac{(m - m')^2}{2\sigma_m^2}\right] dm' dm} \qquad (15)$$

The denominator in this equation is a normalization factor. Given N Einstein ring systems, the total likelihood can be computed as:

$$\mathcal{L}_{tot} = \prod_{j=0}^{N} \mathcal{L}(n_j, \mathbf{m_j}|\mathbf{p}, \mathbf{q}), \qquad (16)$$

with n_j and $\mathbf{m}_j$ the number and masses of subhaloes detected in the jth system.

We perform a MCMC fitting to the mock lens systems. The model has 5 free parameters: $\mathbf{q} = \{\alpha, f_E, M_{ring}, \beta, m_c\}$. In the likelihood function, f_E and M_{ring} are completely degenerate and so they cannot be determined separately using subhalo number counts. In a real observation, the strong lensing image can be used to determine the total mass within

the thin annulus around the Einstein ring region and the stellar mass of the central galaxy can be obtained from multiband photometry. Combining these two masses fixes M_{ring}. Here, we simply set M_{ring} to the value obtained from the MCMC.

As mentioned earlier, the SHMF in CDM follows a power law in mass of exponent, $\alpha = 1.9$ (Springel et al. 2008; Gao et al. 2012). We therefore adopt a Gaussian prior for α with expectation 1.9 and standard deviation 0.1. We also adopt a Gaussian prior for β (Eq. 5) with expectation 1.3 and standard deviation 0.1.

5 RESULTS

Fig. 2 shows the results of the MCMC analysis using 100 mock systems constructed using parameters appropriate to COCO-WARM. Here, the input SHMF is obtained from Eq. 5 with $m_c = 1.3 \times 10^8 h^{-1} M_\odot$. The detection limit was set to $M_{low} = 10^7 h^{-1} M_\odot$. The contours show the 68% and 95% confidence levels for the 2D posterior probability distribution of model parameters, while their marginalized 1D posterior probability distributions are shown as histograms at the end of each row. The red vertical lines show the input value of each parameter. The 2D contours indicate that the parameters, f_E (the fraction of dark matter mass in subhaloes within the Einstein radius), and, m_c (the cutoff mass), are slightly degenerate. That is to say, the lack of small haloes in WDM can be partialy compensated for by a decrease in the overall amplitude of the SHMF. With a detection limit of $M_{low} = 10^7 h^{-1} M_\odot$ and $N = 100$ systems, both m_c and f_E are tightly constrained. Crucially, we find that with data like these one can rule out at the 2σ level all dark matter models with $m_c < 5 \times 10^7 h^{-1} M_\odot$, which includes CDM.

We now explore how the number of strong lens systems, N, affects the constraining power of the method. In Fig. 3, we show constraints on f_E and m_c using 20, 100 and 1000 mock systems for detection limits of $M_{low} = 10^7 h^{-1} M_\odot$ and $M_{low} = 10^8 h^{-1} M_\odot$. The 1σ error on f_E decreases by about a factor of 3 as N increases from 20 to 100. However, even with $N = 20$ lenses, one can still set a clear lower limit of $5 \times 10^7 h^{-1} M_\odot$ for m_c, as long as subhaloes as massive as $M_{low} = 10^7 h^{-1} M_\odot$ can be detected.

The variation of the constraints on m_c for different values of M_{low} is displayed in Fig. 4. Red, black and blue histograms show the marginalized 1D posterior probablity distribution of m_c, for detection limits of $M_{low} = 10^7 h^{-1} M_\odot$, $M_{low} = 10^8 h^{-1} M_\odot$ and $M_{low} = 10^9 h^{-1} M_\odot$ respectively. A detection limit of $M_{low} = 10^9 h^{-1} M_\odot$ hardly constrains the properties of the dark matter. This is not only because of poor detectability, but also because the number of subhaloes above this mass that can be found within a host halo is intrinsically small. For $M_{low} = 10^8 h^{-1} M_\odot$, dark matter models with $m_c < 10^7 h^{-1} M_\odot$ are disfavoured, but are still consistent within the 2σ confidence level. Our results illustrate the vital importance of the subhalo detection threshold in distinguishing different dark matter models.

Lovell et al. (2014) resimulated four WDM analogues of the CDM galactic haloes in the AQUARIUS simulations (Springel et al. 2008) for warmer models than COCO-WARM, specifically for models with power spectrum cutoffs corresponding to thermal relic warm particle masses
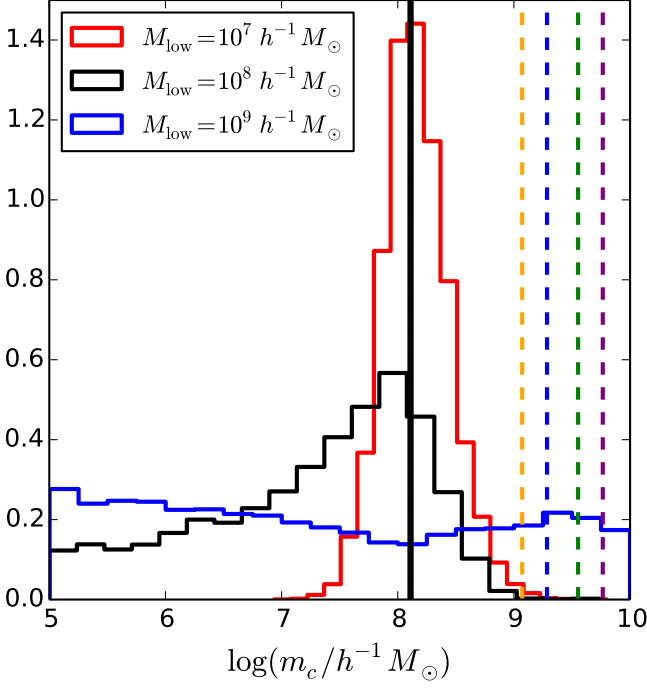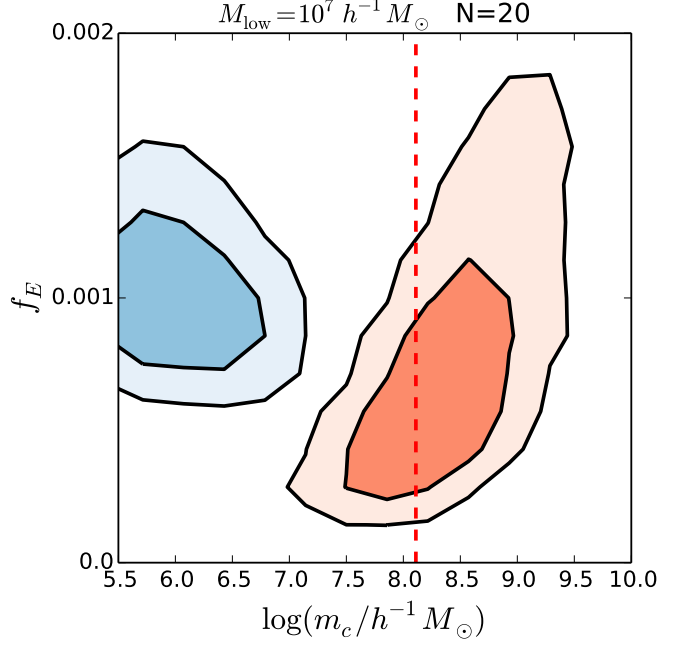
Figure 4. The marginalized 1D probability distribution of m_c for different detection mass limits with $N = 100$. The mock systems are generated using COCO-WDM subhalo mass function. The vertical black solid line shows the m_c value of the COCO-WARM simulation. The coloured dashed lines from left to right show the m_c values of warm dark matter models with particle masses $m_{\rm WDM} = 2.28, 1.95, 1.59, 1.41$ keV respectively.

Figure 5. The 2D posterior probability distribution of f_E and m_c, assuming $N = 20$, $M_{\rm low} = 10^7 h^{-1} {\rm M_\odot}$. The red contour shows the results with input model of COCO-WARM (red), and the blue contour shows the results with input mode of COCO-COLD (blue). The vertical dashed line shows the m_c value of the COCO-WARM simulation.

of $m_{\rm WDM} = [2.28, 1.96, 1.59, 1.41]$ keV. By fitting Eq. 5 to the SHMF in each case, we can obtain values for m_c, which increase for decreasing values of $m_{\rm WDM}$. We find best-fit values of $\log[m_c/(h^{-1}{\rm M_\odot})] = [9.07, 9.28, 9.55, 9.76]$ for $m_{\rm WDM} = [2.28, 1.96, 1.59, 1.41]$ keV respectively. These values are overplotted as the dashed black lines in Fig. 4. It can be seen that with $M_{\rm low} = 10^8 h^{-1}{\rm M_\odot}$ one can set a strong lower limit to $m_{\rm WDM}$.

Finally, in Fig. 5 we show the 2D posterior probability distributions of f_E and m_c using input models of COCO-WARM(red) and COCO-COLD (blue), with $N = 20$ and a detection limit of $M_{\rm low} = 10^7 h^{-1}{\rm M_\odot}$. Encouragingly, we find that this observational set up is sufficient to distinguish between the two cosmologies. In other words, by observing approximately 20 strong lens systems with a detection threshold of $M_{\rm low} = 10^7 h^{-1}{\rm M_\odot}$, we could potentially rule out the 3.3 keV thermal WDM model, which, as discussed earlier, has a very similar power spectrum to the "coldest" 7 keV sterile neutrino model. This is therefore a promising way potentially to rule out the entire family of 7 keV sterile neutrinos as candidates for the dark matter.

6 SUMMARY AND DISCUSSION

In this paper we have investigated the potential of strong gravitational lensing as a diagnostic of the identity of the dark matter. Two of the currently most plausible elementary particle candidates for the dark matter, CDM and WDM,

make very different predictions for the number of low-mass subhaloes that survive within larger haloes by the present day. Strong lensing is sensitive to precisely this population since subhaloes can produce measurable distortions to Einstein rings.

To explore the extent to which strong lensing can constrain the subhalo mass function, we have performed Monte-Carlo simulations to mimic observations of haloes hosting the subhalo mass functions of the COCO-WARM and COCO-COLD high-resolution N-body simulations. The former has a power spectrum appropriate for a 3.3 keV thermal relic, which happens to be a very good approximation to the power spetrum of the *coldest* WDM model which is consistent with a sterile neutrino decay interpretation of the 3.5 keV X-ray line recently discovered in galaxies and clusters (Bulbul et al. 2014; Boyarsky et al. 2014)[2]. Since the free-streaming cutoff wavelength in the linear power spectrum of WDM density fluctuations scales inversely with the mass of the particle, ruling out this model by detecting subhaloes of mass below the mass corresponding to the cutoff scale, would also rule out all other sterile neutrino models compatible with the X-ray line.

The subhalo mass function in COCO-WARM begins to fall below the subhalo mass function of COCO-COLD at a mass of $\sim 10^9 h^{-1}{\rm M_\odot}$. The difference between the two mass functions grows to a factor of two at $10^8 h^{-1}{\rm M_\odot}$, and to an order of magnitude at $10^7 h^{-1}{\rm M_\odot}$.

---

[2] This model is also consistent with current constraints on the number of small-mass haloes at high redshift derived from the Lyman-α forest (Viel et al. 2013).
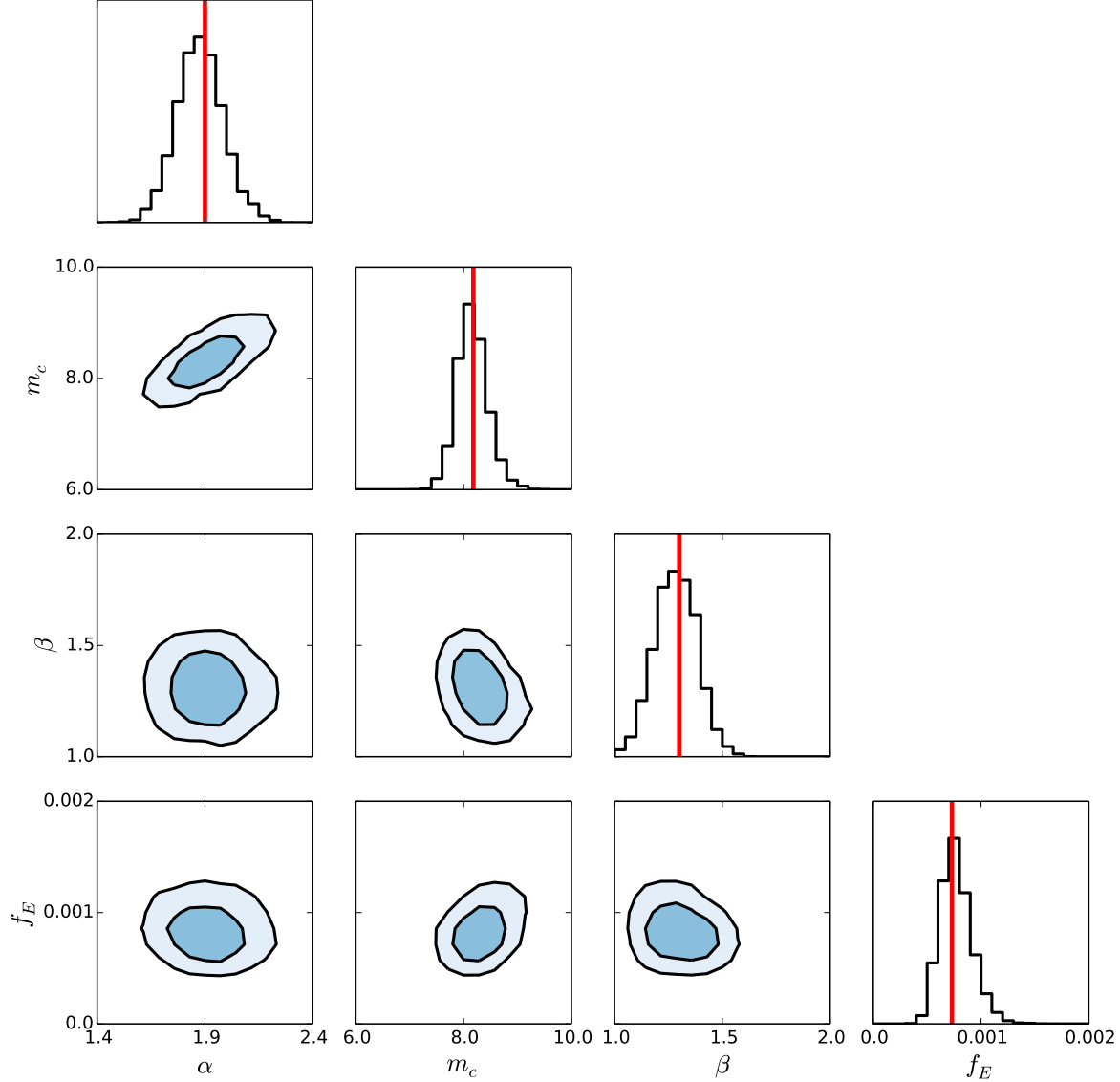
Figure 2. Parameter constraints from 100 mock systems constructed using parameters appropriate to the COCO-WARM simulation. The contours show the 68% and 95% confidence levels for the 2D posterior probability distribution of the model parameters. The histograms at the end of each row show the marginalized 1D posterior probability distribution for each model parameter. The red vertical lines show the input values of each model parameter. The assumed detection limit is $M_{\rm low} = 10^7 h^{-1} {\rm M_\odot}$.

Our analysis, shows that both the subhalo detection limit, $M_{\rm low}$, and the number of observed strong lensing systems are the key for constraining the dark matter model. Specifically, we have shown that a sample of approximately 20 Einstein ring systems with detection limit, $M_{\rm low} = 10^7 h^{-1} {\rm M_\odot}$, is enough clearly to distinguish between the subhalo mass functions of COCO-WARM and COCO-COLD. In other words, if we live in a universe in which the dark matter predominantly consists of 7 keV sterile neutrinos, this test would conclusively rule out CDM, whereas if we live in

a universe in which the dark matter predominantly consists of CDM, the test would rule out all 7 keV sterile neutrino families. If the detection limit is $10^8 h^{-1} {\rm M_\odot}$, the test with about 100 lenses can still set a lower limit on the WDM particle mass, but it cannot rule out CDM at more than 2σ. We stress, however, that tests assuming a more realistic sensitivity function (see Vegetti et al. 2014) are required for a precise result.

Our results highlight the enormous potential for dark matter research of high resolution imaging surveys to search
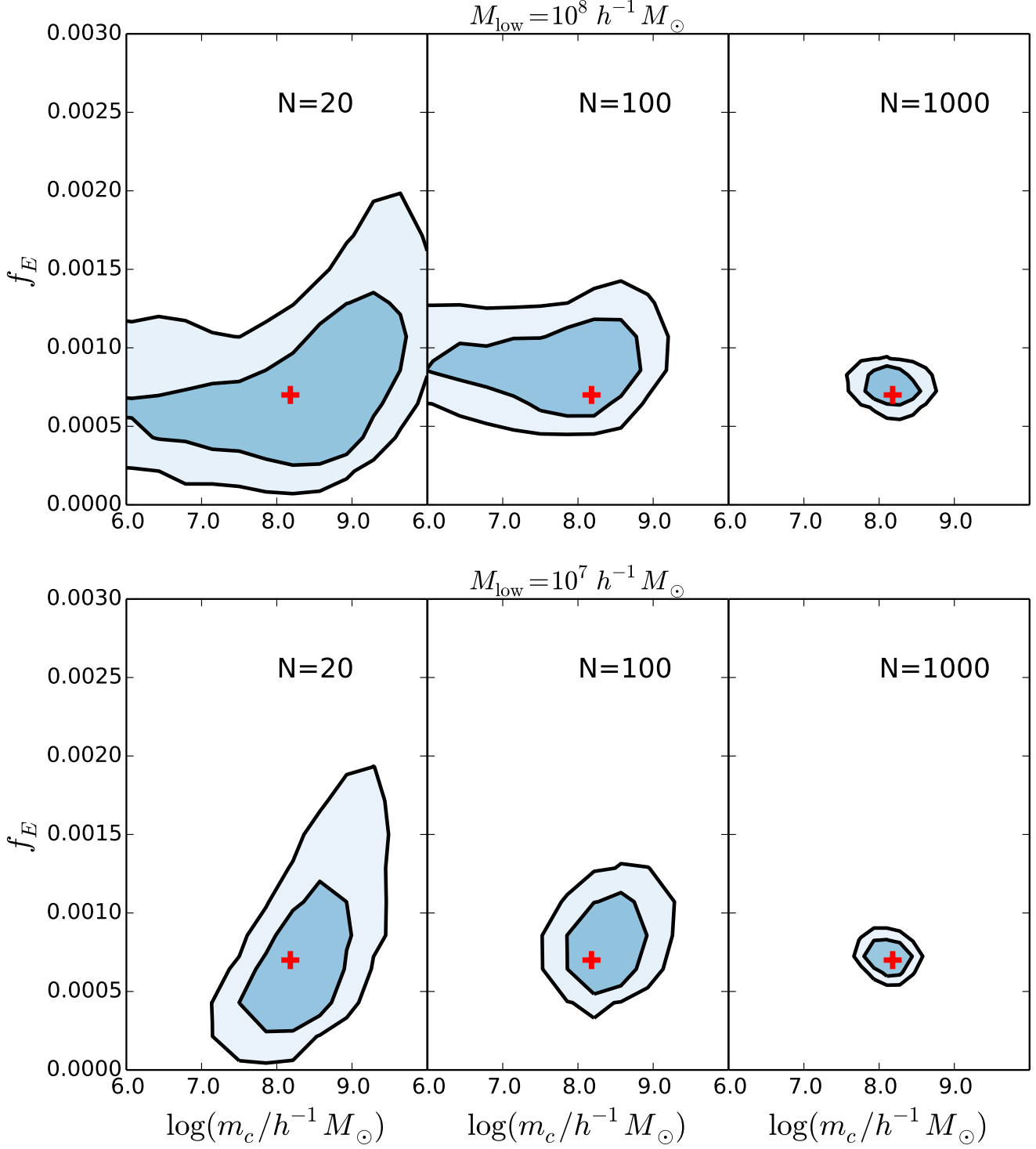
Figure 3. The constraining power on f_E and m_c using 20, 100 and 1000 mock Einstein ring systems. The upper panels show results for $M_{\rm low} = 10^8 h^{-1} {\rm M}_\odot$, while the lower panels show results $M_{\rm low} = 10^7 h^{-1} {\rm M}_\odot$. The input SHMF is from COCO-WARM. The red crosses show the parameter values of COCO-WARM.

for strong lensing systems. Current optical surveys have found $\sim 10^2$ strong lenses, but only a fraction of them have sufficiently high quality data for a measurement of the subhalo mass function. A few subhaloes of mass below $10^9 h^{-1} {\rm M}_\odot$ have already been detected (Vegetti et al. 2010,

2012, 2014). Currently, the lowest subhalo mass detected in an Einstein ring, which was imaged at the Keck telescope, is $1.9 \pm 0.1 \times 10^8 {\rm M}_\odot$ (Vegetti et al. 2012). These authors claim that the detection sensitivity of data of this quality

can reach $2 \times 10^7 \mathrm{M}_\odot$. This is the level required to carry out the test described in this paper.

Planned ground-based telescopes such as LSST and space missions such as Euclid will increase the sample of strong lenses by several orders of magnitude. Euclid, for example, may be able to obtain high resolution images for $\sim 10^5$ strong lenses. At the same time, the SKA survey will increase the sample of strong radio lenses also to $\sim 10^5$. Follow-up observations with VLBI may even detect $10^6 h^{-1} \mathrm{M}_\odot$ subhaloes (McKean et al. 2015). Aside from direct or indirect detection of the dark matter particles themselves, Einstein ring systems currently offer the best astrophysical test of the nature of the dark matter.

REFERENCES

Angulo R. E., Hahn O., Abel T., 2013, MNRAS, 434, 3337

Avila-Reese V., Colín P., Piccinelli G., Firmani C., 2003, ApJ, 598, 36

Bode P., Ostriker J. P., Turok N., 2001, ApJ, 556, 93

Bolton A. S., Burles S., Koopmans L. V. E., Treu T., Moustakas L. A., 2006, ApJ, 638, 703

Bose S., Hellwing W. A., Frenk C. S., Jenkins A., Lovell M. R., Helly J. C., Li B., 2015, ArXiv e-prints

Boyarsky A., Ruchayskiy O., Iakubovskyi D., Franse J., 2014, Physical Review Letters, 113, 251301

Boyarsky A., Ruchayskiy O., Shaposhnikov M., 2009, Annual Review of Nuclear and Particle Science, 59, 191

Bulbul E., Markevitch M., Foster A., Smith R. K., Loewenstein M., Randall S. W., 2014, ApJ, 789, 13

Cautun M., Hellwing W. A., van de Weygaert R., Frenk C. S., Jones B. J. T., Sawala T., 2014, MNRAS, 445, 1820

Cole S., Percival W. J., Peacock J. A., Norberg P., Baugh C. M., Frenk C. S., Baldry I., Bland-Hawthorn J., 2005, MNRAS, 362, 505

Colín P., Avila-Reese V., Valenzuela O., 2000, ApJ, 542, 622

Czoske O., Barnabè M., Koopmans L. V. E., Treu T., Bolton A. S., 2008, MNRAS, 384, 987

Davis M., Efstathiou G., Frenk C. S., White S. D. M., 1985, ApJ, 292, 371

Frenk C. S., White S. D. M., 2012, Annalen der Physik, 524, 507

Gao L., Frenk C. S., Boylan-Kolchin M., Jenkins A., Springel V., White S. D. M., 2011, MNRAS, 410, 2309

Gao L., Navarro J. F., Frenk C. S., Jenkins A., Springel V., White S. D. M., 2012, MNRAS, 425, 2169

Gerhard O., Kronawitter A., Saglia R. P., Bender R., 2001, AJ, 121, 1936

Han J., Cole S., Frenk C. S., Jing Y., 2015, ArXiv e-prints

Hellwing W. A., Frenk C. S., Cautun M., Bose S., Helly J., Jenkins A., Sawala T., Cytowski M., 2015, ArXiv e-prints

Hooper D., Goodenough L., 2011, Physics Letters B, 697, 412

Jenkins A., 2013, MNRAS, 434, 2094

Kochanek C. S., 1991, ApJ, 373, 354

Komatsu E., Smith K. M., Dunkley J., Bennett C. L., Gold B., Hinshaw G., Jarosik N., Larson D., 2010, ArXiv e-prints

Koopmans L. V. E., 2005, MNRAS, 363, 1136

Koopmans L. V. E., Treu T., Bolton A. S., Burles S., Moustakas L. A., 2006, ApJ, 649, 599

Li R., Mo H. J., Fan Z., Yang X., Bosch F. C. v. d., 2013, MNRAS, 430, 3359

Li R., Shan H., Mo H., Kneib J.-P., Yang X., Luo W., van den Bosch F. C., Erben T., Moraes B., Makler M., 2014, MNRAS, 438, 2864

Lovell M. R., Bertone G., Boyarsky A., Jenkins A., Ruchayskiy O., 2015, MNRAS, 451, 1573

Lovell M. R., Eke V., Frenk C. S., Gao L., Jenkins A., Theuns T., Wang J., White S. D. M., Boyarsky A., Ruchayskiy O., 2012, MNRAS, 420, 2318

Lovell M. R., Frenk C. S., Eke V. R., Jenkins A., Gao L., Theuns T., 2014, MNRAS, 439, 300

Mao S., Schneider P., 1998, MNRAS, 295, 587

McAlpine S., Helly J. C., Schaller M., Trayford J. W., Qu Y., Furlong M., Bower R. G., Crain R. A., 2015, ArXiv e-prints

McKean J., Jackson N., Vegetti S., Rybak M., Serjeant S., Koopmans L. V. E., Metcalf R. B., Fassnacht C., Marshall P. J., Pandey-Pommier M., 2015, Advancing Astrophysics with the Square Kilometre Array (AASKA14), p. 84

Metcalf R. B., Madau P., 2001, ApJ, 563, 9

Peebles P. J. E., 1982, ApJL, 263, L1

Planck Collaboration Ade P. A. R., Aghanim N., Armitage-Caplan C., Arnaud M., Ashdown M., Atrio-Barandela F., Aumont J., Baccigalupi C., Banday A. J., et al. 2014, A&A, 571, A16

Riemer-Sorensen S., 2014, ArXiv e-prints

Schaye J., Crain R. A., Bower R. G., Furlong M., Schaller M., Theuns T., Dalla Vecchia C., 2015, MNRAS, 446, 521

Schneider A., Smith R. E., Macciò A. V., Moore B., 2012, MNRAS, 424, 684

Springel V., 2005, MNRAS, 364, 1105

Springel V., Wang J., Vogelsberger M., Ludlow A., Jenkins A., Helmi A., Navarro J. F., Frenk C. S., 2008, MNRAS, 391, 1685

Springel V., White S. D. M., Frenk C. S., Navarro J. F., Jenkins A., Vogelsberger M., Wang J., Ludlow A., Helmi A., 2008, Nature, 456, 73

Springel V., White S. D. M., Tormen G., Kauffmann G., 2001, MNRAS, 328, 726

Tegmark M., Strauss M. A., Blanton M. R., Abazajian K., Dodelson S., Sandvik H., Wang X., 2004, PhRevD, 69, 103501

Vegetti S., Koopmans L. V. E., 2009a, MNRAS, 392, 945

Vegetti S., Koopmans L. V. E., 2009b, MNRAS, 400, 1583

Vegetti S., Koopmans L. V. E., Auger M. W., Treu T., Bolton A. S., 2014, MNRAS, 442, 2017

Vegetti S., Koopmans L. V. E., Bolton A., Treu T., Gavazzi R., 2010, MNRAS, 408, 1969

Vegetti S., Lagattuta D. J., McKean J. P., Auger M. W., Fassnacht C. D., Koopmans L. V. E., 2012, Nature, 481, 341

Viel M., Becker G. D., Bolton J. S., Haehnelt M. G., 2013, PhRevD, 88, 043502

Viel M., Lesgourgues J., Haehnelt M. G., Matarrese S., Riotto A., 2005, PhRevD, 71, 063534

Wang J., White S. D. M., 2007, MNRAS, 380, 93

Xu D., Sluse D., Gao L., Wang J., Frenk C., Mao S., Schneider P., Springel V., 2015, MNRAS, 447, 3189

Xu D. D., Mao S., Wang J., Springel V., Gao L., White S. D. M., Frenk C. S., Jenkins A., Li G., Navarro J. F., 2009, MNRAS, 398, 1235